Superconducting properties and microstructures for Ba_2SmNbO_6 and $BaHfO_3$ co-doped $SmBa_2Cu_3O_y$ thin films

Yuma Kusafuka[1], Yusuke Ichino[1], Yuji Tsuchiya[1], Ataru Ichinose[2], Yuatka Yoshida[1]

[1]Department of Energy Engineering and Science, Nagoya University, Furo-cho, Chikusa-ku, Nagoya 464-8603, Japan
[2]Electric Power Engineering Research Laboratory, Central Research Institute of Electric Power Industry, Yokosuka, Kanagawa 240-0196, Japan

Corresponding author:
Y. Ichino, Ph. D.
Department of Energy Engineering and Science, Nagoya University
Furo-cho, Chikusa-ku, Nagoya 464-8603, Japan

Phone: +81-52-789-3908
e-mail: ichino@nuee.nagoya-u.ac.jp

Abstract

Recently, we observed that Ba_2SmNbO_6 (BSNO), which has double perovskite structure, formed wide nanorods in a $SmBa_2Cu_3O_y$ (SmBCO) film compared with $BaHfO_3$ (BHO) nanorods. These wide nanorods could trap flux quanta under low magnetic fields effectively. On the other hand, narrow nanorods could trap flux quanta under high magnetic fields. In this paper, we doped SmBCO films with both of BSNO and BHO in aiming to introduce both of wide and narrow nanorods to bring out the flux pinning property at low and high magnetic fields simultaneously. We investigated their microstructures and superconducting properties. As a result, we confirmed that wide and narrow nanorods coexisted in the SmBCO films. Each of wide and narrow nanorods trapped flax quanta at different magnetic fields. Also, we explored optimal composition for the BSNO+BHO co-doped SmBCO films. These findings indicate that flux pinning properties can be tuned by multiple doping of BMO materials.

1 Introduction

Introducing artificial pinning centers into $REBa_2Cu_3O_y$ is effective to enhance superconducting properties under magnetic fields [1]. Especially, $BaMO_3$ (M= Zr, Sn, Hf, etc.) and Ba_2REMO_6 (RE=rare earth, M=Nb, Ta, etc.) forms nanorods inside the $REBa_2Cu_3O_y$ matrix and these barium based metal oxides are abbreviated as BMO in this paper. The BMO nanorods are useful pinning centers for trapping magnetic fields applied parallel to the *c*-axis [2-6]. Controlling nanorods diameter and number density are important for improving superconducting properties, because pinning properties of the film with nanorods depends on their shapes [7]. Number density of nanorods increases with increasing BMO content [8]. Much nanorods density is desirable to enhance superconducting properties under high magnetic fields, but excessive BMO content induces a decline of superconducting properties [9]. A lot of reports about controlling nanorods shape have been published, for example the dependence of substrate temperature, laser frequency and a kind of BMO materials [10-12], complex microstructure has been established such as multilayered structure, and a structure with both of nanorods and nanoparticles [13, 14]. Especially, we reported that high flux pinning force density of 1.6 TN/m^3 at 4.2 K in a $BaHfO_3$-doped SmBCO film deposited at low substrate temperature of 720ºC [15].

Flux pinning in $REBa_2Cu_3O_y$ films is affected by BMO nanorod shape such as diameter, number density of and inclination angle for normal direction of substrate surface. Because a diameter of vortex is affected by temperature, a valid diameter of pinning centers is also affected by temperature. For example, pinning centers with large diameter contributes to pin flux line at a high temperature. Number density of nanorods affects to a matching field, namely, high number density of nanorods leads to a high matching field of a $REBa_2Cu_3O_y$ film. When nanorods direction is parallel to an applied magnetic field, nanorods show maximum flux pinning force. Therefore, BMO nanorod shape is important to control flux pinning properties in $REBa_2Cu_3O_y$ films.

Recently, we have reported that Ba_2SmNbO_6 (BSNO) in a $SmBa_2Cu_3O_y$ (SmBCO) thin film forms the widest nanorods of the diameter of 35 ± 6 nm among other BMO nanorods, and the film showed distinctive superconducting properties in magnetic fields such as a peak effect in magnetic field dependence of critical current density (J_c) and a strange irreversibility line with “reverse S” shape [16]. These peculiar properties are observed at high measurement temperatures around critical temperature, because the BSNO nanorods with large diameter of 35 nm strongly contribute to the flux pinning at the high measurement temperature due to enlarged vortex diameter at the temperature.

Determinant factors for nanorod diameters are investigated by some groups. Wu et al. reported that diameter of $BaZrO_3$ (BZO) nanorods in YBCO films was able to be calculated from energetic minimum of elastic energies induced by lattice strain between BZO and YBCO [17]. Based on crystal growth theory, we developed a Monte Carlo simulation of a BMO doped $REBa_2Cu_3O_y$ system, and we clarified effects of various deposition parameters such as substrate temperature, deposition rate and BMO content on morphologies of BMO nanostructures [18-20]. As a result, BMO self-organized into diverse nanostructures depending on the deposition parameters, and number density of the nanostructures increased with decreasing substrate temperature, increasing deposition rate and BMO content. In other words, wide nanorods, which correspond to low number density at a certain BMO content, would be formed at high substrate temperature and low deposition rate. Surely, the wide BSNO nanorods in the SmBCO film also grew at relatively high T_s of 880ºC and low v_{dr} of 50 nm/h. One can expect that BMO nanorods with low number density and wide diameter are effective for flux pinning at low magnetic fields.

On the other hand, $BaHfO_3$ (BHO) in a SmBCO film formed a narrow nanorods of 13.5 nm as compared with the BSNO-doped film, although the BHO-doped SmBCO film was deposited at high T_s of 940ºC [12]. It indicates that diameter of BMO nanorods is also affected by a kind of BMO material. The narrow BHO nanorods shows excellent J_c in high magnetic fields.

In this paper, we doped both of BSNO and BHO into SmBCO films aiming to form both narrow and wide nanorods to bring out the flux pinning property at low and high magnetic fields simultaneously, and we investigated their microstructures and superconducting properties.

2 Experimental procedure

In this study, SmBCO films were fabricated by PLD method with Nd:YAG laser (λ=266 nm) at a repetition rate of 2 Hz on (100) LAO single crystalline substrates. The laser energy density and distance between a substrate and targets were 2.0 J/cm^2 and 42.5 mm, respectively. The films were grown at a substrate temperature of 880ºC at an O_2 partial pressure of 400 mTorr, and film thickness was about 300 nm. BSNO and BHO were doped in the SmBCO films by an alternating targets technique because it can easily control BMO content [21]. In all the BSNO and BHO co-doped films, BSNO content was fixed to 32vol.%, and BHO content was varied from 5.2 to 10.5vol.%, in which 32vol.% of BSNO was fixed, by controlling targets alternating cycle as shown in Fig. 1. BHO content is controlled by the pulse number X which is a range from 4 to 11.

We abbreviate a co-doped SmBCO film with 32vol.% of BSNO and *x*vol.% of BHO to BSNO+BHO(*x*)-SmBCO. Also, a BSNO 32vol.% doped film and a BHO 8.5vol.% doped film are written as BSNO-SmBCO and BHO-SmBCO, respectively. The samples were fabricated by the same deposition condition for comparison with BSNO+BHO(*x*)-SmBCO. The orientation and *c*-axis length of the films were characterized by X-ray diffraction (XRD) with CuKα radiation. Compositions of the films were measured by scanning electron microscopy with energy dispersive X-ray spectroscopy. Microstructure of the films was observed by transmission electron microscopy (TEM), and nanorods diameters and number density were measured from plane view TEM images. The superconducting properties were measured by physical property measurement system using a standard four-probe method. Critical temperature (T_c) and J_c were defined from *R*-*T* and *I*-*V* curves with electric field criterion of 1.0 μV/cm. Irreversibility fields were determined from the *R*-*T* curves at various magnetic fields.

3. Results and discussion

At first, we evaluated microstructures and J_c in magnetic fields of a BSNO-SmBCO and a BHO-SmBCO. Fig. 2(a) shows a plane view image of transmission electron microscopy (TEM) of the BSNO-SmBCO. These diameter and number density were about 32 ± 4 nm and 285 /μm^2, respectively. One can see that dark circular contrast around the nanorods. Because of lattice mismatch between SmBCO and BSNO, there is strain field around the interface. Therefore, the circular contrast corresponds to the strain filed. On the other hand, the BHO-SmBCO fabricated by the same deposition condition with the BSNO-SmBCO had narrow and high number density of nanorods as shown in Fig. 2(b). These diameter and number density were about 12 ± 2 nm and 1300/μm^2, respectively. These TEM images clearly show that the BSNO-SmBCO includes wider nanorods as compared with the BHO-SmBCO. Fig. 3 shows magnetic field dependence of J_c for pure-SmBCO, the BHO-SmBCO and the BSNO-SmBCO at 77 K under magnetic fields applied parallel to the *c*-axis of SmBCO. The BSNO-SmBCO has plateau with a range from 0.2 T to 0.4 T. That indicates wide BSNO nanorods trap flux quanta under low magnetic fields effectively, but not effective in high magnetic fields because of their low number density. On the other hand, the BHO-SmBCO has plateau with a range from 1.0 T to 2.5 T. That indicates narrow BHO nanorods are good for trapping flux quanta under high magnetic fields because of their high number density.

We prepared a SmBCO film co-doped with 32vol.% BSNO and 8.5vol.% BHO

[BSNO+BHO(8.5)-SmBCO] at the same deposition conditions. Figs. 4(a) and (b) shows the plane view and cross-sectional TEM images of BSNO+BHO(8.5)-SmBCO. We observed wide and narrow nanorods separately. Each of nanorods grew vertically from the substrate to the film surface as shown in Fig. 4(b). This indicate that we succeed to control the microstructure as mentioned in introduction. Figs. 4(c) and (d) shows EDX elemental mappings for Hf and Nb of Fig. 4(a). We observed that there are both Hf and Nb in wide and narrow nanorods. From these figures, the wide nanorods include both Nb and Hf. On the other hand, the narrow nanorods consist of mainly Hf and a small amount of Nb is also included. This indicates that BSNO and BHO partly mix because crystal structure of BSNO is similar to that of BHO. Actually, wide and narrow nanorods were mainly composed by BSNO and BHO, respectively. We can observe similar strain field around wide nanorods with Fig. 2(a), and this fact also supports that the wide nanorods mainly consists of BSNO.

Fig. 5 shows the histogram of nanorod diameters for the BSNO+BHO(8.5)-SmBCO. Table 1 shows average diameter and number density estimated from Fig. 5, those of the BSNO-SmBCO and the BHO-SmBCO are also listed for comparison. The average nanorod diameters for wide and narrow nanorods in the BSNO+BHO(8.5)-SmBCO were 29 ± 4 nm and 7.5 ± 0.9 nm, and that of number density were 388 /μm^2 and 175 /μm^2, respectively. The diameter and the number density of narrow nanorods decreased as compared with the BHO-SmBCO, because a part of BHO was absorbed into wide nanorods. On the other hand, the average diameter of wide nanorods was almost the same with the BSNO-SmBCO, and number density increased compared with the BSNO-SmBCO because BMO doping level increased due to absorption of BHO into wide nanorods, consequently.

T_c and *c*-axis length of SmBCO matrix for the samples are listed in the table 1. It is considered that T_c decrease by doping BMO due to a lattice stress between a SmBCO and the lattice stress extends *c*-axis length of SmBCO. The T_c for the BHO-SmBCO was relatively low owing to high BHO content, since we controlled it as same BHO content as in the BSNO+BHO(8.5)-SmBCO. Additionally, all the films fabricated under same deposition condition which is optimal for the BSNO+BHO(8.5)-SmBCO. On the other hand, we did not observe particular decline of T_c for the BSNO-SmBCO as compared with that of pure SmBCO, and *c*-axis lengths of SmBCO for the films were almost the same. These facts indicate that BSNO doping, which is equal less than at least 32vol.%, hardly affects on T_c because lattice stress of the SmBCO matrix induced by BSNO nanorods would be negligible. Although this mechanism of low lattice stress has not been clarified yet, one of the reasons would be low number density of the BSNO

nanorods. Interface area of SmBCO matrix and BSNO nanorods decreases with decreasing the number density, so that lattice stress becomes low. In BSNO+BHO(8.5)-SmBCO, because total number density of wide and narrow nanorods were higher than BSNO-SmBCO, T_c and *c*-axis lengths of SmBCO were lower and higher than those of the BSNO-SmBCO, respectively. As the result, interface area of SmBCO matrix and nanorods increased. Namba et al. reported that interface areas of $ErBa_2Cu_3O_y$ and nanorods controlled T_c of various BMO-doped films [22], and the report supports our results.

Fig. 6(a) shows magnetic field dependence of J_c for the samples at 77 K under magnetic fields applied parallel to *c*-axis of the films. We observed the BSNO+BHO(8.5)-SmBCO had double plateaus with ranges from 0.2 T to 0.5 T and from 1.0 to 1.5 T. The plateau under lower magnetic field was slightly longer than that of the BSNO-SmBCO because the wide nanorod density in the BSNO+BHO(8.5)-SmBCO was larger than that in the BSNO-SmBCO. On the other hand, the plateau under higher magnetic field was shorter than that in the BHO-SmBCO because the narrow nanorod density was less than that in the BHO-SmBCO. Fig. 6(b) shows magnetic field dependence of F_p calculated from Fig. 6(a). It shows the BSNO+BHO(8.5)-SmBCO had shoulder at 0.7 T indicated by a black arrow in the figure, and the shoulder was almost the same with a matching field estimated from the number density of the wide nanorods. The maximum F_p for the BSNO+BHO(8.5)-SmBCO was 20.7 GN/m^3 at 2.0 T which was higher than those of BSNO-SmBCO and BHO-SmBCO. These results indicate that each of wide and narrow nanorods trapped flax quanta at the different magnetic fields in spite of coexistence of these nanorods, and that led to high performance of F_p.

Fig. 7 shows irreversibility fields (B_{irr}s) at various temperatures for the films. We observed a peak around 0.5 T in the BSNO+BHO(8.5)-SmBCO. Similar behavior is observed in the BSNO-SmBCO. We reported the same peculiar B_{irr} line in a BSNO-doped SmBCO film and concluded that wide and threading nanorods contributed to the peculiar B_{irr} line [16]. These facts indicate that the peaks induced by wide nanorods in the BSNO+BHO(8.5)-SmBCO. Additionally, B_{irr} line of the BSNO+BHO(8.5)-SmBCO shows a kink structure in a range from 0.8 T to 1.1 T which is similar behavior with that of the BHO-SmBCO. Here, 0.8 T corresponds to a matching field for only wide nanorods, while 1.1 T is identical to a matching field for total amount of wide and narrow nanorods in the film. From above results, we conclude that wide nanorods trapped flax quanta at low magnetic fields, and both wide and narrow nanorods are effective at high magnetic fields.

In order to explore optimal composition for the BSNO+BHO co-doped films, we controlled BHO content. Fig. 8 shows magnetic field dependence of J_c for BSNO+BHO(x)-SmBCO films (x=5.2~10.5vol.%) at 77 K under magnetic fields applied parallel to c-axis of these films. There is no plateau in the BSNO+BHO(5.2)-SmBCO under high magnetic fields. Almost of BHO could be absorbed into wide nanorods. On the other hands, the films with x of more than 7.2vol.% had double plateaus, that indicates that the films include both wide and narrow nanorods and the number density of the nanorods is enough to improve J_c at high magnetic fields. The BSNO+BHO(7.2)-SmBCO showed shorter plateau under higher magnetic fields compared with the BSNO+BHO(8.5)-SmBCO. This result indicated that increasing BHO content was effective to increase of number density of narrow nanorods. From the results of Figs. 6 and 8, we find that the distinctive J_c double plateau reflects the microstructure of the films with two types of diameters of nanorods.

However, J_c at self-field for the BSNO+BHO(10.5)-SmBCO decreased because of their excessive BHO content. As a result, optimal BHO content was 8.5vol.% for a BSNO 32vol.%+ BHO co-doped film. Furthermore, these findings suggest that a J_c-B curve can be tuned by adding several kinds of BMO materials.

4. Conclusion

In order to enhance superconducting properties under both low and high magnetic fields, we doped BSNO and BHO into SmBCO films aiming to form both narrow and wide nanorods by pulsed laser deposition method adopting alternating targets technique. As a result, we observed both wide and narrow nanorods in a BSNO+BHO(8.5)-SmBCO. The average nanorods diameters for wide and narrow nanorods were 30 and 7.5 nm, and that of number density were 388 /μm^2 and 175 /μm^2, respectively. Each of nanorods preferentially trapped flax quanta under low and high magnetic fields, respectively. The F_p^{max} for the BSNO+BHO(8.5)-SmBCO was 20.7 GN/m^3 at 2 T which was higher than those of the BSNO-SmBCO and the BHO-SmBCO.

And also, we tried to explore for optimal BHO content for BSNO+BHO co-doped films. As a result, a film with small BHO content did not show plateau under high magnetic fields. On the other hand, excessive BHO content induced decline of J_c at self-field. In this study, optimal BHO content was 8.5vol.% for the BSNO 32vol.%+ BHO co-doped film.

Although separate growth mechanism of wide and narrow nanorods has not been clarified yet, above results indicate that flux pinning properties can be tuned by multiple

doping of BMO materials.

Acknowledgments

This work was partly supported by a Grant-in-Aid for Scientific Research (15H04252, 15K14301, 15K14302 and 16K20898), NU-AIST alliance project and JST-ALCA.

References

[1] Mele P, Matsumoto K, Hride T, Ichinose A, Mukaida M, Yoshida Y, Horii S, Kita R 2008 *Supercond. Sci. Technol.* **21** 032002

[2] Macmanus-Driscoll J L, Foltyn S R, Jia Q X, Wang H, Serquis A, Maiorov B, Civale L, Hawley M E, Maley M P, Peterson D E 2004 *Nature Materials* **3** 439

[3] Varanasi C V, Burke J, Bunke L, Wang H, Sumption M, Barnes P N 2007 *J. Appl. Phys.* **102** 63909

[4] Tobita H, Notoh K, Higashikawa K, Inoue M, Kiss T, Kato T, Hirayama T, Yoshizumi T, Izumi T, Shiohara Y 2012 *Supercond. Sci. Technol.* **25** 062002

[5] Wee S H, Goyal A, Zuev Y, Cantoni C, Selvamanickam V, Specht E D 2010 *Appl. Phys. Express* **3** 023101

[6] Kai H, Mukaida M, Teranishi R, Mori N, Yamada K, Horii S, Ichinose A, Kita R, Matsumoto K, Yoshida Y, Awaji S, Watanabe K, Namba M, Fujiyoshi T 2008 *Physica C* **468** 1854

[7] Wee H W, Gao Y, Zuev Y L, More K L, Meng J, Zhong J, Stocks G M, Goyal A 2013 *Adv. Funct. Mater.* **23** 1912

[8] Awaji S. Namba M, Watnabe K, Ito S, Aoyagi E, Kai H, Mukaida M, Kita R 2009 *J. Appl. Phys.* **106** 103915

[9] Mele P, Matsumoto K, Ichinose A, Mukaida M, Yoshida Y, Horii S, Kita R 2009 *Physica C* **469** 1380

[10] Haruta M, Ichinose A, Fujita N, Saura K, Maeda K, Horii S 2013 *IEEE Trans. Appl. Supercond.* **23** 8000904

[11] Maiorov B, Baily S A, Zhou H, Ugurlu O, Kennison J A, Dowden O C, Holesinger T G, Folthn S R, Civale L 2009 *Nature Materials.* **6** 398

[12] Tsuruta A, Yoshida Y, Ichino Y, Ichinose A, Matsumoto K, Awaji S 2014 *Supercond. Sci. Technol.* **27** 065001

[13] Tsuruta A, Yoshida Y, Ichino Y, Ichinose A, Matsumoto K, Awaji S 2013 *Jpn. J. Appl. Phys.* **52** 010201

[14] Horide T, Kawamura T, Matsumoto K, Ichinose A, Yoshizumi M, Izumi T, Shiohara Y 2013 *Supercond. Sci. Technol.* **26** 075019

[15] Miura S, Yoshida Y, Ichino Y, Xu Q, Matsumoto K, Ichinose A, Awaji S 2016 *APL Mater.* **4** 016102

[16] Ichino Y, Kusafuka Y, Ichinose A, Yoshida Y 2017 *Jpn. J. Appl. Phys.* **56** 073101

[17] Wu J Z, Shi J J, Baca J F, Emergo R, Haugan T J, Maiorov B, Holesinger T 2014 *Supercond. Sci. Technol.* **27** 044010

[18] Ichino Y, Tsuruta A, Miura S, Yoshida Y, Yoshizumi M, Izumi T 2015 *IEEE Trans.*

Appl. Supercond. **25** 6604506
[19] Ichino Y, Yoshida Y, Miura S 2017 *Jpn. J. Appl. Phys.* **56** 015601
[20] Ichino Y, Yoshida Y 2017 *IEEE Trans. Appl. Supercond.* **27** 7500304
[21] Haugan T, Barnes P N, Maartense I, Cobb C B 2003 *J. Mater. Res.* **18** 2618
[22] Namba M, Awaji S, Watanabe K, Ito S, Aoyagi E, Kai H, Mukaida M, Kita R 2009 *Appl. Phys. Express* **2** 073001

Table 1 Comparison between the properties of $SmBa_2Cu_3O_y$ films incorporating Ba_2SmNbO_6 and $BaHfO_3$.

BMO material, Additive amount	BSNO 32vol.% + BHO 8.5vol.%		BSNO 32 vol.%	BHO 8.5 vol.%	pure
	Wide nanorods	Narrow nanorods			
Nanorod diameter [nm]	30 ± 4	7.5 ± 0.9	32 ± 4	12 ± 2	
Number density of nanorods [μm^{-2}]	388	175	285	1300	
T_c [K]	88.9 ± 0.2		91.0 ± 0.2	88.1 ± 0.2	90.7 ± 0.2
c-axis length [Å]	11.81		11.77	11.82	11.77

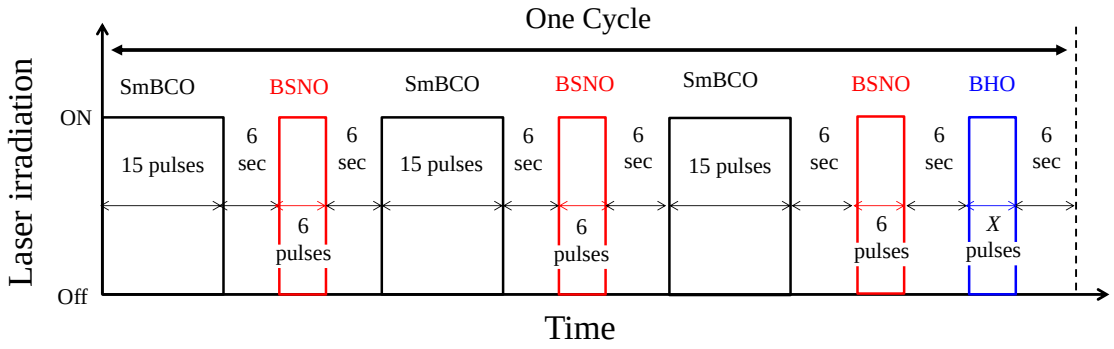

Fig. 1 Targets alternating cycle and irradiation pulse number for SmBCO, BSNO and BHO targets.

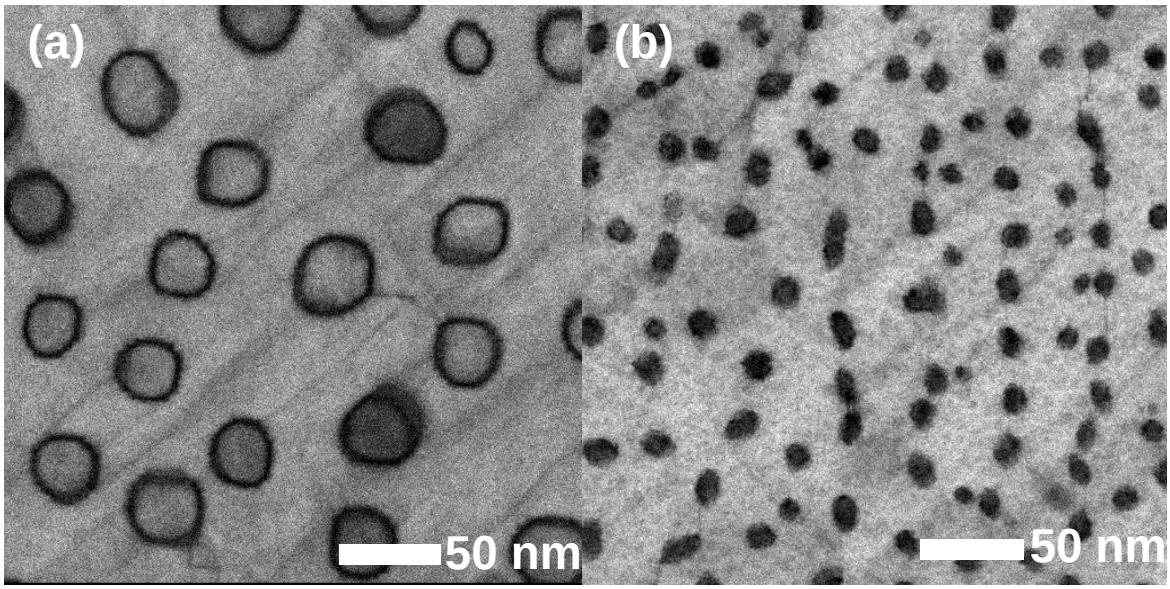

Fig. 2 Planer view of TEM images for (a) BSNO 32vol.%-doped SmBCO film, (b) BHO 8.5vol.%-doped SmBCO film.

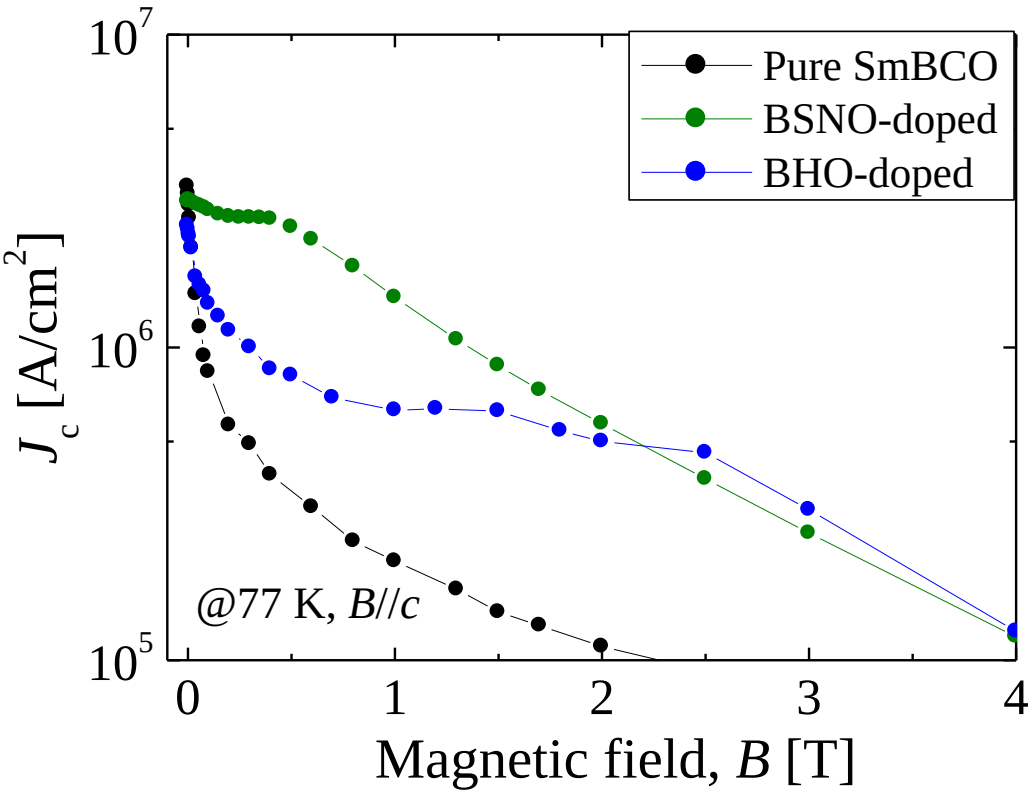

Fig. 3 Magnetic field dependence of J_c for pure, BHO 8.5vol.%-doped and BSNO 32vol.%-doped SmBCO films at 77 K under magnetic fields applied parallel to the *c*-axis of SmBCO.

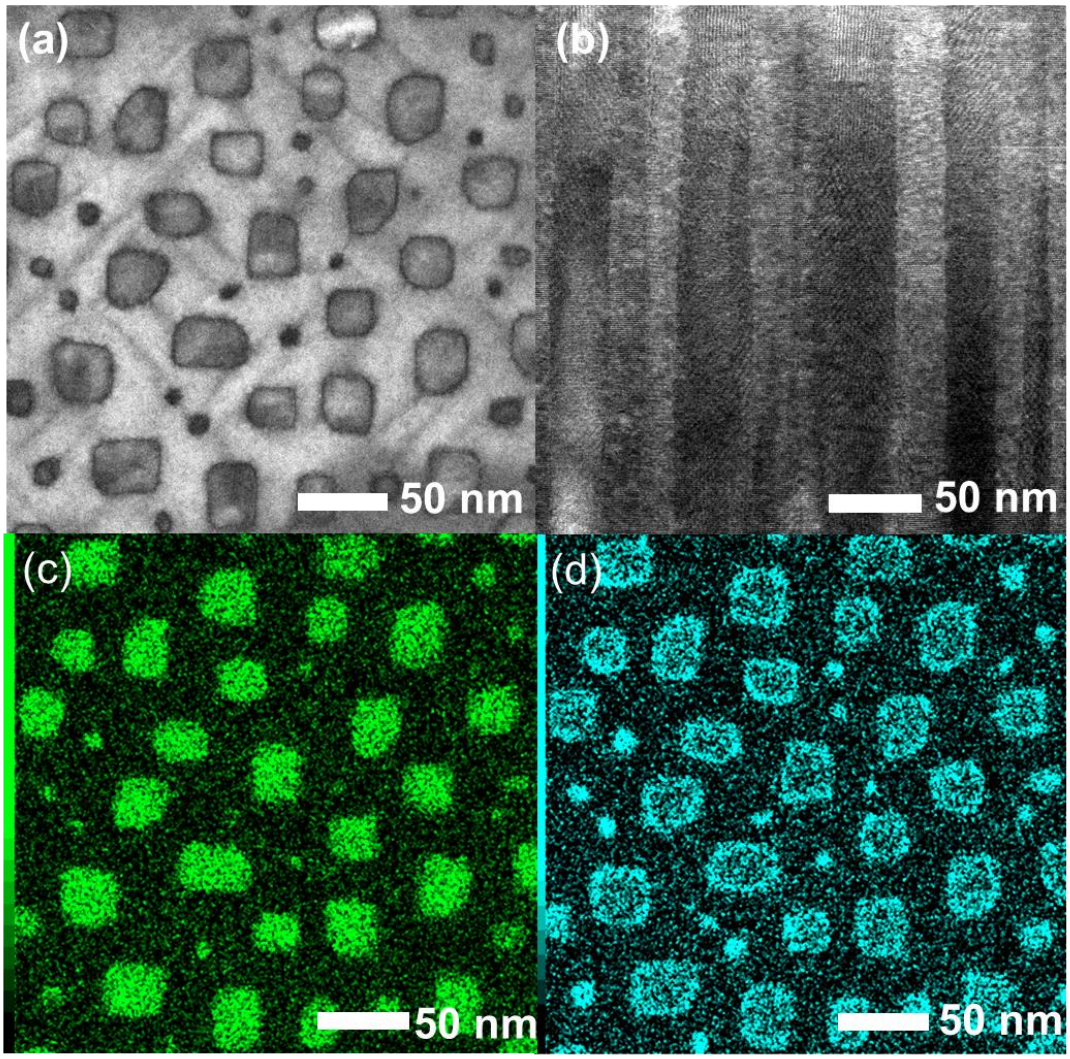

Fig. 4 (a) Plane view and (b) cross-sectional TEM images of BSNO 32vol.% and BHO 8.5vol.% co-doped SmBCO film. EDX elemental mappings of (c)Nb and (d) Hf for the plane view image.

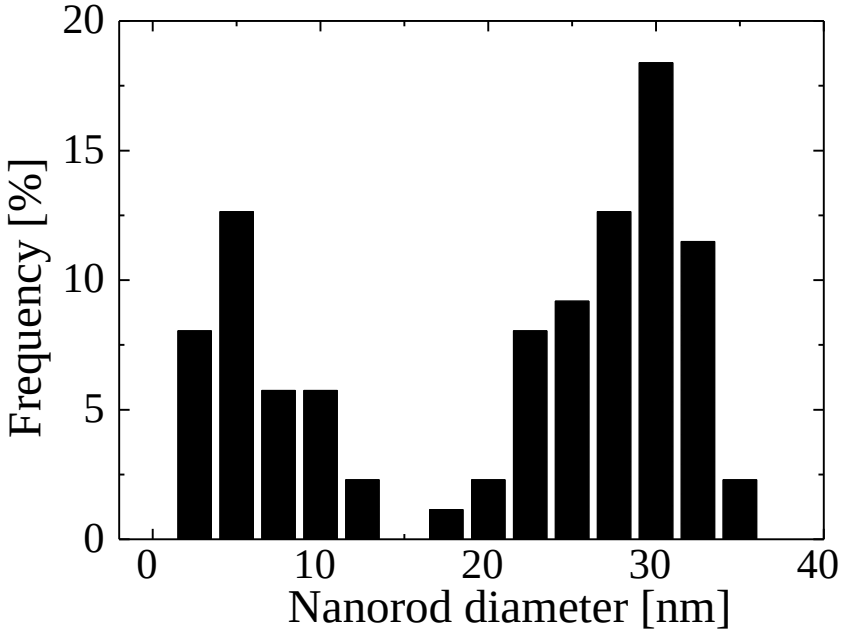

Fig. 5 Histogram of nanorod diameters for the SmBCO film co-doped with BSNO 32vol.% and BHO 8.5vol.%.

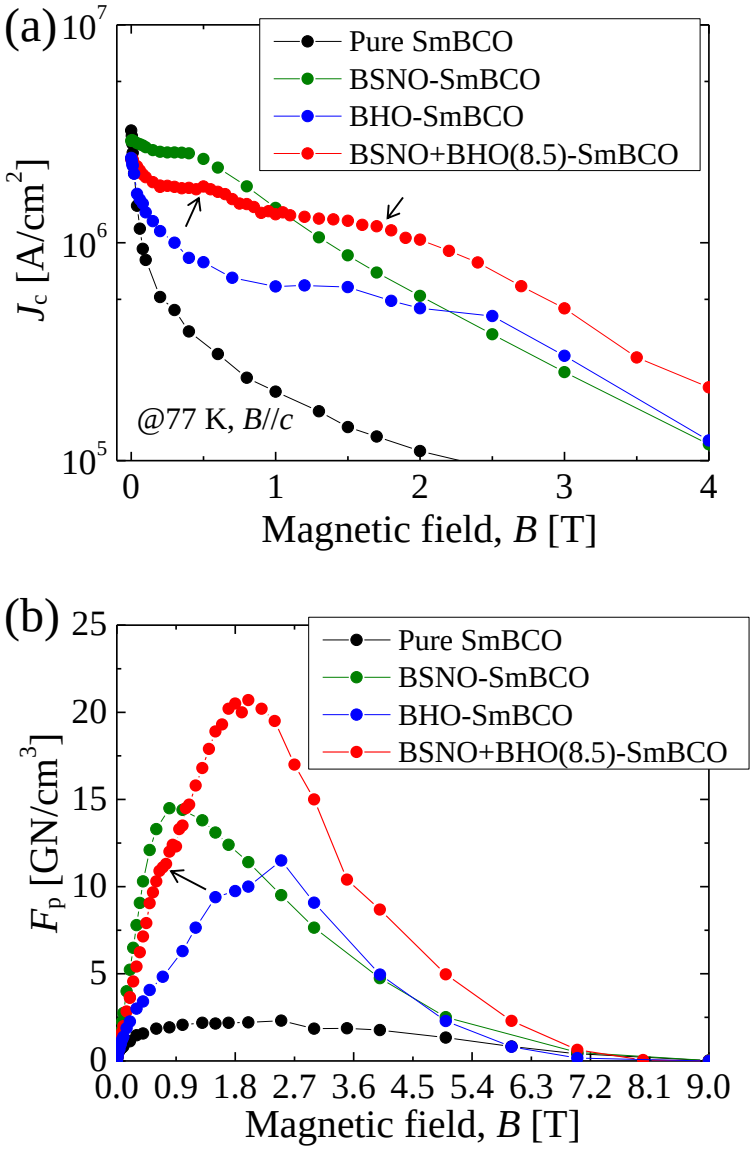

Fig. 6 Magnetic field dependence of (a)J_c and (b)F_p for pure, BSNO 32vol.%-doped, BHO 8.5vol.%-doped, BSNO 32vol.%+BHO 8.5vol.% co-doped SmBCO films at 77 K under magnetic fields applied parallel to the *c*-axis of SmBCO. In (a), the co-doped film shows a double J_c plateau, and end fields of the double plateau are pointed out by arrows in (a). A black arrow in (b) shows a shoulder at 0.7 T.

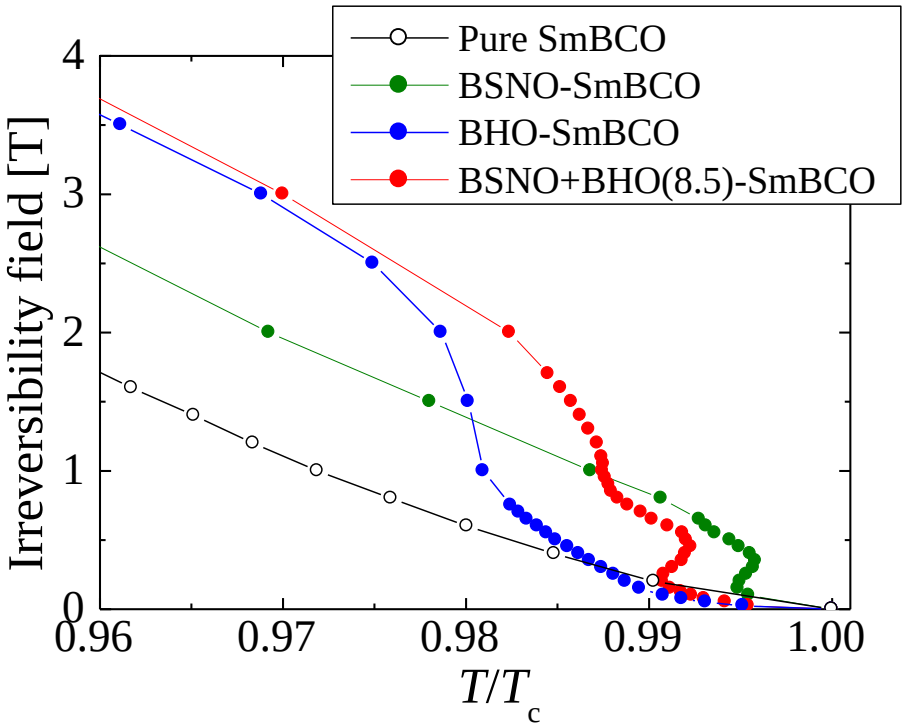

Fig. 7 Temperature dependence of irreversibility fields. Horizontal axis is normalized by each T_c at 0 T.

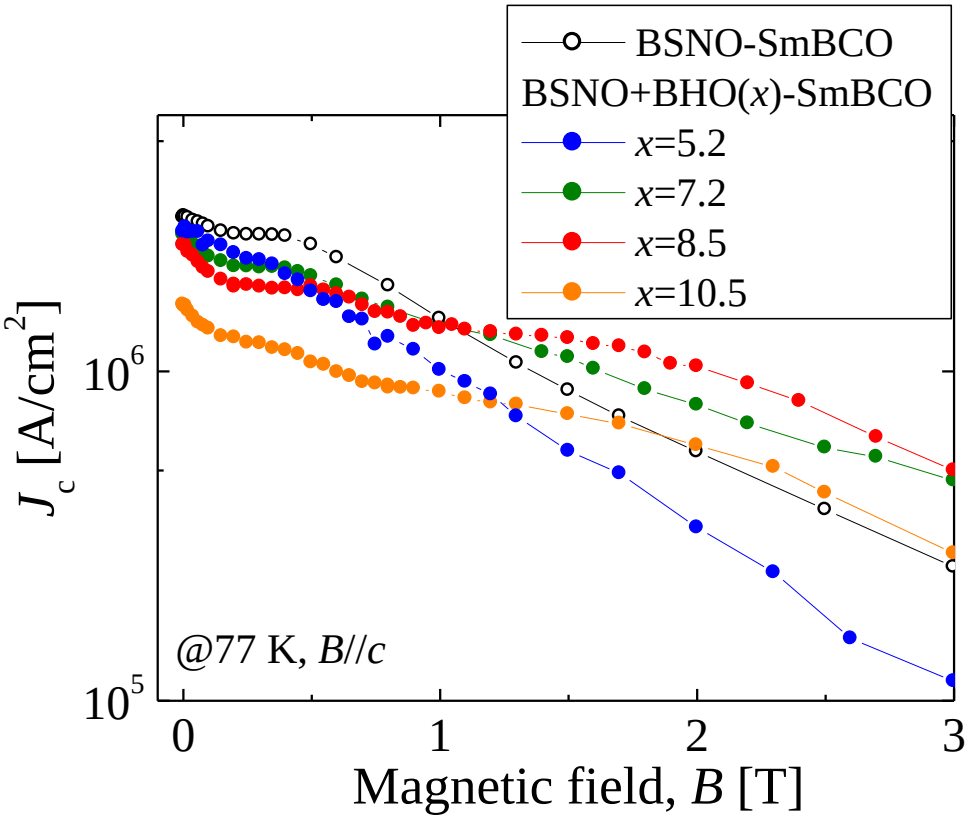

Fig. 8 Magnetic field dependence of J_c for BSNO 32vol.%+ BHO 5.2-10.5vol.% co-doped SmBCO films at 77 K under the fields applied parallel to *c*-axis of SmBCO.